LIMNOLOGY and OCEANOGRAPHY

ASLO

Limnol. Oceanogr. 9999, 2024, 1–14

doi: 10.1002/lno.12534

Variability in the phytoplankton response to upwelling across an iron limitation mosaic within the California current system

YuanYu Lin,[1] **Olivia Torano**,[1] **Logan Whitehouse**,[1] **Emily Pierce**,[1,2] **Claire P. Till**,[3] **Matthew Hurst**,[3] **Robert Freiberger**,[3,4] **Travis Mellett**,[5] **Maria T. Maldonado**,[6] **Jian Guo**,[6] **Mariam Sutton**,[1] **David Zeitz**,[7] **Adrian Marchetti**[1*]

[1]Department of Earth, Marine, and Environmental Sciences, University of North Carolina, Chapel Hill, North Carolina, USA
[2]Department of Marine, Earth, and Atmospheric Sciences, North Carolina State University, Raleigh, North Carolina, USA
[3]Department of Chemistry, California State Polytechnic University, Arcata, California, USA
[4]Scripps Institute of Oceanography, University of California, San Diego, California, USA
[5]School of Oceanography, University of Washington, Seattle, Washington, USA
[6]Department of Earth, Ocean, and Atmospheric Sciences, University of British Columbia, Vancouver, British Columbia, Canada
[7]Department of Chemistry and Biochemistry, University of California, Santa Cruz, California, USA

Abstract

Coastal upwelling currents such as the California Current System (CCS) comprise some of the most productive biological systems on the planet. Diatoms dominate these upwelling events in part due to their rapid response to nutrient entrainment. In this region, they may also be limited by the micronutrient iron (Fe), an important trace element primarily involved in photosynthesis and nitrogen assimilation. The mechanisms behind how diatoms physiologically acclimate to the different stages of the upwelling conveyor belt cycle remain largely uncharacterized. Here, we explore their physiological and metatranscriptomic response to the upwelling cycle with respect to the Fe limitation mosaic that exists in the CCS. Subsurface, natural plankton assemblages that would potentially seed surface blooms were examined over wide and narrow shelf regions. The initial biomass and physiological state of the phytoplankton community had a large impact on the overall response to simulated upwelling. Following on-deck incubations under varying Fe physiological states, our results suggest that diatoms quickly dominated the blooms by "frontloading" nitrogen assimilation genes prior to upwelling. However, diatoms subjected to induced Fe limitation exhibited reductions in carbon and nitrogen uptake and decreasing biomass accumulation. Simultaneously, they exhibited a distinct gene expression response which included increased expression of Fe-starvation induced proteins and decreased expression of nitrogen assimilation and photosynthesis genes. These findings may have significant implications for upwelling events in future oceans, where changes in ocean conditions are projected to amplify the gradient of Fe limitation in coastal upwelling regions.

Eastern boundary upwelling currents (EBUC), while comparatively smaller in size to other regions of the ocean, are disproportionately some of the most productive ecosystems on the planet (Carr 2001; Capone and Hutchins 2013). Characterized by equatorward wind patterns that result in a net offshore transport of surface water and the upwelling of cold nutrient-rich water from below (Huyer 1983), these regions provide for extensive phytoplankton blooms that not only support the local food web but also mediate the flux of carbon into the deep ocean (Capone and Hutchins 2013). The California Current system (CCS), one such EBUC, is particular in its irregular bathymetry and seasonality, where the frequency of upwelling is enhanced more often during the spring and summer (Closset et al. 2021). The unusual qualities of the CCS are furthermore pronounced by its Fe limitation mosaic (Hutchins et al. 1998; Bruland et al. 2001), in which regions with wide and shallow continental shelves are mostly considered Fe-

*Correspondence: amarchetti@unc.edu

Additional Supporting Information may be found in the online version of this article.

Author Contribution Statement: Study conception and design: YuanYu Lin and Adrian Marchetti. Data collection: YuanYu Lin, Adrian Marchetti, Olivia Torano, Logan Whitehouse, Emily Pierce, Claire P. Till, Matthew Hurst, Robert Freiberger, Travis Mellett, Maria T. Maldonado, Jian Guo and Miriam Sutton. Analysis and interpretation of results: YuanYu Lin, Adrian Marchetti, Olivia Torano, Emily Pierce, Claire P. Till, and Maria T. Maldonado. Analysis for supporting information: YuanYu Lin, Adrian Marchetti, Claire P. Till, and David Zeitz. Draft Manuscript preparation: YuanYu Lin and Adrian Marchetti. All authors reviewed and approved the results as well as the final version of this manuscript.

replete, while those with narrow and deeper continental shelves have been found to experience Fe limitation of phytoplankton growth (Bruland et al. 2001). This is explained by the fact that wide and shallow continental shelves act as Fe traps (Capone and Hutchins 2013). During the upwelling season, Fe-rich sediments from the bottom are more likely entrained into surface waters to seed phytoplankton blooms, while there is an inadequate supply of Fe to complement high macronutrient concentrations in narrow shelf regions because upwelling is focused off the shelf and over the deeper continental slope (Bruland et al. 2001; Capone and Hutchins 2013). Occasionally when these trends are not observed, it is usually due to mesoscale features such as eddies moving water that was recently upwelled inland of the shelf offshore, or vice versa (Till et al. 2019).

Within this complex system lies a sequence of idealized light and nutrient zones (Fig. 1A). On the surface, upwelled phytoplankton physiologically acclimate to optimal light and nutrient conditions (high light and high nutrients) and accelerate nitrogen rate processes relative to carbon rate processes, leading to enhanced macromolecule synthesis and growth referred to as "shift-up" (Wilkerson and Dugdale 1987). The increased algal growth processes exhibited during this stage is matched by the increase of their biomass and the formation

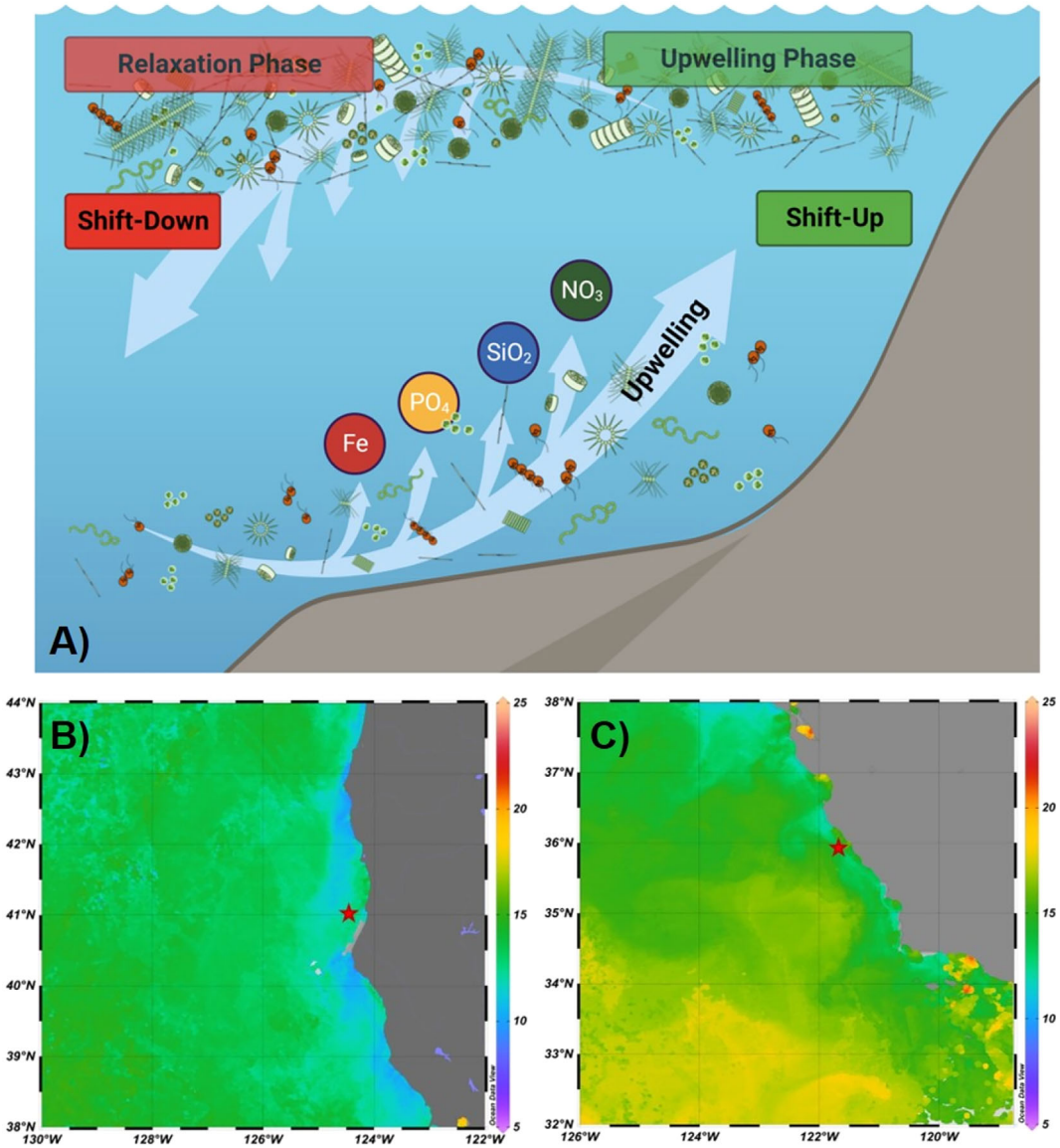

Fig. 1. (**A**) Conceptual model of the upwelling conveyor belt cycle (UCBC) in upwelling systems and the idealized zones within the upwelling cycle. Image modified from Lampe et al. (2021). Remote sensing imagery (14-day averages) of SST in the (**B**) wide shelf and (**C**) narrow shelf regions at the time of collection. Red stars on each map denote the respective location of deep-water collection for the incubation experiments. Remote-sensing data were derived from NOAA CoastWatch program.

of phytoplankton blooms. By maintaining high transcript abundances of nitrogen assimilation genes even in the seed populations, diatoms can ensure a more rapid physiological response to upwelling compared to other phytoplankton taxa. This advantageous "frontloading" of nitrogen assimilation machinery allows them to rapidly dominate these blooms in coastal upwelling areas (Lampe et al. 2018), and as noted by Margalef's Mandala principle (Margalef 1978), exhibit high specific growth rates and thrive under high turbulence (upwelling). A course of succession follows as other phytoplankton taxonomic groups exhibit a slower reaction and response to the upwelling. As nutrient concentrations are rapidly depleted (high light and low nutrients), the cells undergo a "shift-down" response, in which rate processes decrease further downstream. Phytoplankton will sink throughout this cycle, and may be re-upwelled in the next upwelling event (Wilkerson and Dugdale 1987). Naturally, phytoplankton seed populations are established from the sinking communities as they are advected offshore. During this stage, the aging waters may be increasingly nitrate limited, and cells increase their C : N ratios above that of the Redfield ratio (6.6 C : 1 N) as they sink below the euphotic zone. Once at depth (low light and high nutrients), diatoms are set apart by the differential expression of nitrogen transporters and other nitrogen assimilation genes compared to other phytoplankton taxa (Lampe et al. 2021).

Upwelling-simulation studies conducted in the laboratory have recently shown an increase in the relative expression of nitrogen assimilation genes in the dark (simulated sinking out of the euphotic zone) in the diatom *Chaetoceros decipiens*, while the coccolithophore, *Emiliania huxleyi* showed a relatively lower expression of the same genes in the dark, further supporting the diatom "frontloading" hypothesis for N assimilation (Lampe et al. 2021). Ultimately, diatoms can ensure a more rapid physiological response to upwelling compared to other phytoplankton taxa. Once they are upwelled, diatoms may rapidly increase growth through enhanced nitrogen metabolism and continue building up photosynthetic machinery until nitrate depletion or sinking. This highly dynamic series of physical and biological phases is defined as the upwelling conveyor belt cycle. In essence, upwelled diatoms employ a proactive approach and maintain elevated pools of these nitrogen-related genes throughout the upwelling conveyor belt cycle, whereas other phytoplankton employ a more reactive approach and upregulate primary nitrate assimilation genes post-upwelling. This distinctive molecular strategy to constitutively express nitrogen assimilation genes is believed to provide these diatom taxa with a physiological edge in their "shift-up" response to upwelling (Lampe et al. 2021).

Iron (Fe) is yet another nutrient that differentially influences phytoplankton growth and community composition. It is an important micronutrient found in the photosynthetic reaction centers (photosystems I and II), and is vital to both oxygenic photosynthesis and ATP synthesis (Falkowski 1997; Marchetti and Maldonado 2016). Furthermore, Fe plays a significant role in nitrogen assimilation, where the assimilatory enzymes nitrate reductase (NR) and nitrite reductase (NiR) both contain Fe. Fe is a limiting nutrient to productivity in vast offshore regions of the ocean, as phytoplankton subjected to low Fe availability have both experienced reductions in photosynthetic rates as well as NiR activity (Milligan and Harrison 2000). Fe bioavailability further influences Fe uptake, storage and conservation mechanisms in phytoplankton (see Supporting Information Data S2.11). Most of the dissolved Fe is complexed to organic ligands (Gledhill and Buck 2012; Hutchins and Boyd 2016), but a small amount of the unchelated labile Fe (III)—or Fe′—is found to be the most readily available source of Fe for phytoplankton (Turnšek et al. 2019).

This study aims to understand the complexity of the phytoplankton response to the upwelling conveyor belt cycle, and simultaneously examine their physiological and transcriptomic changes in relation to Fe status within the CCS. The primary focus of this research is predicated on how Fe limitation can change and shape natural phytoplankton community structure, and how it plays a role in their acclimation to the upwelling conveyor belt cycle with the understanding that future coastal oceans are likely to experience dramatic shifts in Fe bioavailability across different topographical regions. Three central questions are addressed: (1) How does Fe limitation change the phytoplankton community structure, physiological response to upwelling, and gene expression of different phytoplankton groups during an upwelling event? (2) In what ways are diatoms responding to fluctuations in Fe bioavailability with respect to the upwelling conveyor belt cycle and topographical variation? (3) How much impact do diatom seed populations impose on their ability to respond to an upwelling event, and what are the biological driving forces that aid in their acclimation to upwelling?

Methods

Experimental design

The primary objective of this study was to observe how subsurface phytoplankton communities respond to the upwelling conveyor belt cycle. To capture this phenomenon, we conducted on-deck incubations that spanned different time points which represented the different stages of growth (initial deep-water community at T_0, and stimulated growth phases at T1 and T2). We further subjected the incubations to various Fe-related treatments to test how Fe might play a role in determining their physiological and molecular response to upwelling. Ultimately, the incubations allowed us to examine and track the growth of the CCS phytoplankton communities through a simulated upwelling experiment.

Sample sites

The first incubation was conducted from 27 May to 01 June 2019. The site (41°0′52.956″N and 124°24′58.68″W) was

located off the coast of northern California over a wide continental shelf (Supporting Information Fig. S1). Upwelling conditions were not present at this site during the initial collection for the incubation experiment on May 27th. Sea surface temperature (SST) data obtained from remote sensing before, during, and after this wide shelf incubation suggests that upwelling had ceased ~ 11 d prior to the collection, and the site was in a period of relaxation throughout the incubation experiment (Fig. 1B).

The second incubation was conducted from 02 June to 06 June 2019. The site (35°55′24.7074″N and 121°32′34.44″W) was located in the Big Sur region of central California and characterized by a narrow continental shelf (Supporting Information Fig. S1) where Fe is historically thought to be low (Bruland et al. 2001). SST data for the narrow shelf incubation at Big Sur indicated that the region had not experienced an upwelling event for over a month prior to the experiment, but was transitioning to upwelling conditions prior to our occupation and was in an upwelling state during the incubation experiment (Fig. 1C).

For this experiment, we simulated upwelling by pumping water from the isotherm range that would bring nutrient-rich cold water to the surface once upwelling favorable conditions were reinstated. Water temperatures within the 8–10°C isotherms were used as the threshold. Satellite-derived data for SST was obtained from NOAA POES AVHRR satellite (NOAA/NESDIS Center for Satellite Applications Research), downloaded from the NOAA CoastWatch Browser and plotted with GraphPad Prism v9.2.0.

Water collection and incubation

Seawater was collected using trace-metal clean techniques from a depth of 90 m (corresponding to the 8.4°C isotherm) for the wide shelf incubation and 80 m (corresponding to the 8.9°C isotherm) for the narrow shelf incubation. Seawater from both sites was pumped directly into a positive pressure trace metal clean plastic bubble created in the ship's laboratory into large, 50-gal acid-washed high-density polyethylene (HDPE) drums to homogenize the seawater using a Wilden air-operated double-diaphragm pump made of polytetrafluoroethylene and acid-washed HDPE tubing. Preparation of the cubitainers was carried out prior to the cruise and included trace-metal clean techniques (Crawford et al. 2003): cubitainers were initially soaked in 2% Extran detergent for 7 d, then rinsed with deionized water four times and Milli-Q water three times prior to being soaked in 10% reagent grade hydrochloric acid for 2–3 d and rinsed with Milli-Q water. Subsequently, the cubitainers were soaked in 1% trace metal grade hydrochloric acid for 7 d and rinsed with Milli-Q water, then soaked in 0.1% trace metal grade acetic acid 3–4 d before final storage in low Fe water from Station P (50°N and 145°W). Station P water had been collected and filtered from the 2018 EXPORTS North Pacific field campaign using trace metal clean techniques and stored in the dark at 4°C until use.

In the bubble, these triplicate acid-cleaned 10 L low-density polyethylene cubitainers were filled and then incubated in large on-deck plexiglass incubators circulated with water chilled to the temperatures at which the subsurface samples were collected using Aqua Logic Delta Star® In-Line Water Chillers. Incubators were covered with neutral density screening to achieve 30% incident irradiance. To assess the effects of Fe addition or removal on the simulated upwelled plankton communities, samples were incubated with no amendment (control), amended with 5 nM of $FeCl_2$ (Fe treatment), or amended with 200 nM desferrioxamine B (DFB), a strong Fe chelator, which inhibits dissolved Fe uptake (DFB treatment). Three cubitainers were immediately harvested for the initial timepoint (T_0), also referred to as deep-water or DW. The remaining cubitainers were incubated for two additional timepoints for a total of 18 cubitainers per incubation. Cubitainers were harvested for various biological and chemical parameters (see below) following 48 h (T_1) for both incubation experiments, and following 120 h in the wide shelf incubation and 96 h in the narrow shelf incubation (T_2). Methods used for collection of physiological measurements (Data S1.1), isotopic uptake rate measurements (Data S1.2), and RNA (Data S1.5) are provided in the Supporting Information. Bioinformatic methods used for sequence analysis, including taxonomic and functional annotations and gene expression are provided in Supporting Information Data S1.5. Methods (Data S1.6) and discussion of ANOVA statistical analyses (Data S2.3) are provided in the Supporting Information.

Data deposition

The sequence data reported in this study will be deposited to the National Center for Biotechnology sequence read archive. RNA sequences are under submission no. SUB13179044 and rDNA sequences are under the submission no. SUB12523058 (Bioproject accession no. PRJNA966115). Assembled contigs, read counts, and annotations are deposited to Zenodo. Data for this project was also submitted to BCO-DMO under project number 768006.

Results

Shelf characteristics during water collections

The ambient deep-water communities (DW) incubated for the simulated upwelling experiments were collected at roughly 8.4°C isotherm for the wide shelf (90 m) and 8.9°C isotherm for the narrow shelf (80 m). For the wide shelf seawater, SST data derived from satellite imagery provided evidence that upwelling had ceased 11 d prior to the start of the on-deck incubation, and the site was in a state of relaxation throughout the remainder of the experiment. In contrast, SST data for the narrow shelf suggested that the area was transitioning to upwelling conditions just prior to our occupation, and was in an upwelling state during the on-deck incubation (Supporting Information Fig. S1B). Macronutrient

concentrations in both incubations remained high throughout the incubation, and there is no evidence of macronutrient limitation or depletion at any point during the incubation experiments. Further details on macronutrient drawdown are provided in the Supporting Information Data (S2.1).

Phytoplankton biomass

Chlorophyll *a* (Chl *a*) concentrations were generally lower in the wide shelf relative to that of the narrow shelf incubations. Comparing across sites, the wide shelf incubation started with a relatively lower Chl *a* biomass ($0.019 \pm 0.003\ \mu g\ L^{-1}$, average ± standard deviation) at T_0 compared to that of the narrow shelf incubation ($0.31 \pm 0.05\ \mu g\ L^{-1}$) for the large size-fraction (Supplementary Table S2). Similarly, the initial deep-water community of the small size-fraction in the wide shelf incubation ($0.015 \pm 0.003\ \mu g\ L^{-1}$) was five-fold lower in biomass than that of the narrow shelf ($0.10 \pm 0.01\ \mu g\ L^{-1}$). In the wide shelf incubation, Chl *a* data indicated an increase of large phytoplankton (≥ 5 μm) by T_2 in the control ($0.66 \pm 0.14\ \mu g\ L^{-1}$) and Fe ($0.80 \pm 0.26\ \mu g\ L^{-1}$) treatment, as the DFB treatment ($0.08 \pm 0.04\ \mu g\ L^{-1}$) yielded observably lower biomass relative to the control and Fe treatments (Fig. 2A). For the smaller phytoplankton (< 5 μm), the control ($0.12 \pm 0.09\ \mu g\ L^{-1}$), Fe ($0.09 \pm 0.04\ \mu g\ L^{-1}$), and DFB treatment ($0.04 \pm 0.02\ \mu g\ L^{-1}$) were markedly lower in biomass by T_2 than those of the larger fraction. In the narrow shelf incubation, Chl *a* data also indicated an increase of mostly large phytoplankton by T_2 of the incubation in the control ($10.7 \pm 4.1\ \mu g\ L^{-1}$, average ± standard deviation), Fe ($8.2 \pm 1.4\ \mu g\ L^{-1}$), and DFB ($3.31 \pm 0.47\ \mu g\ L^{-1}$) treatments, although DFB had a noticeable negative effect on biomass accumulation (Fig. 2A). Differences in Chl *a* for the smaller phytoplankton among the control ($0.59 \pm 0.28\ \mu g\ L^{-1}$), Fe ($1.16 \pm 0.35\ \mu g\ L^{-1}$), and DFB ($0.79 \pm 0.07\ \mu g\ L^{-1}$) treatments at T_2 of the narrow shelf incubation are less distinct. Interestingly, DFB did not seem to appreciably influence biomass accumulation of the smaller phytoplankton (Fig. 2B).

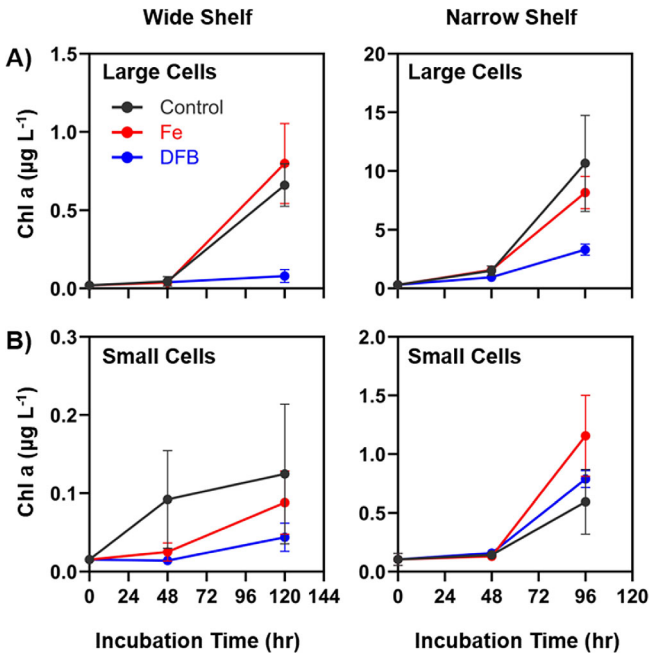

Fig. 2. Chl *a* concentrations over the time course of the wide shelf and narrow shelf incubations for the (**A**) large cell size-fractions (≥ 5 μm) and for the (**B**) small cell size-fraction (< 5 μm). Black, red, and blue circles and lines represent values of the control, Fe, and DFB treatments, respectively. Chl *a* concentrations for the initial deep-water seed communities (T_0) are provided in Supplementary Table S1A. Error bars represent the standard deviations of the mean ($n = 3$).

In the wide shelf incubations, cell counts (Fig. 3A) derived from fluorescence-assisted flow cytometry (FCM) at T_2 show a pronounced increase in diatoms (small diatoms and large centric diatoms) in the control (994 ± 33.6 cells mL^{-1}, small diatom; 184 ± 7.1 cells mL^{-1}, large centric) and Fe treatments (1005 ± 213.4 cells mL^{-1}, small diatom; 209 ± 78.9 cells mL^{-1}, large centric), as the DFB treatment had a noticeable inhibiting effect on diatom growth (270 ± 15.2 cells mL^{-1}, small diatom; 31.8 ± 4.2 cells mL^{-1}, large centric). Neither the small diatoms nor the large centric diatoms displayed any noticeable differences in abundance across the treatments at T_1 of the wide shelf incubation (Fig. 3A). Picoeukaryotes displayed similar patterns to that of the diatoms in the control (66.4 ± 5.2 cells mL^{-1}, T_1; 306.8 ± 110.7 cells mL^{-1}, T_2), Fe (45.7 ± 21.4 cells mL^{-1}, T_1; 213.4 ± 35.6 cells mL^{-1}, T_2), and DFB (8.9 ± 4.1 cells mL^{-1}, T_1; 18.9 ± 7.9 cells mL^{-1}, T_2) treatments, but were noticeably lower in abundances relative to the diatoms. The cyanobacteria *Synechococcus* were found to be more abundant at T_0 in the wide shelf (92.2 ± 3.6 cells mL^{-1}) relative to the rest of the incubation time points, but also displayed DFB treatment effects at both T_1 and T_2 (Fig. 3A). In the narrow shelf, no noticeable difference in small diatom abundances across treatments was observed at T_1 or T_2, although the DFB treatment (636 ± 56.5 cells mL^{-1}) had a negative effect on the population average of large diatoms relative to the control (2690 ± 20.9 cells mL^{-1}) and Fe treatments (2977 ± 390.9 cells mL^{-1}) at T_2 (Fig. 3B). Similar to that of the large diatoms, the population average of picoeukaryotes in the narrow shelf incubation also displayed a DFB treatment effect (927 ± 71.0 cells mL^{-1}) relative to the control (2827 ± 807.1 cells mL^{-1}) and Fe treatments (3834 ± 189.5 cells mL^{-1}) at T_2, while no noticeable difference was observed at T_1. The *Synechococcus* population was also found to be more abundant at T_0 (250 ± 8.9 cells mL^{-1}) compared to the rest of the incubation time points, but did not show a DFB treatment effect at T_2 (Fig. 3B).

Inorganic carbon and nitrate uptake rates

Biomass-normalized dissolved inorganic carbon (DIC; $0.0018 \pm 0.001\ h^{-1}$) and nitrate ($0.0038 \pm 0.0019\ h^{-1}$) uptake of the large cell (≥ 5 μm) deep-water (T_0) community

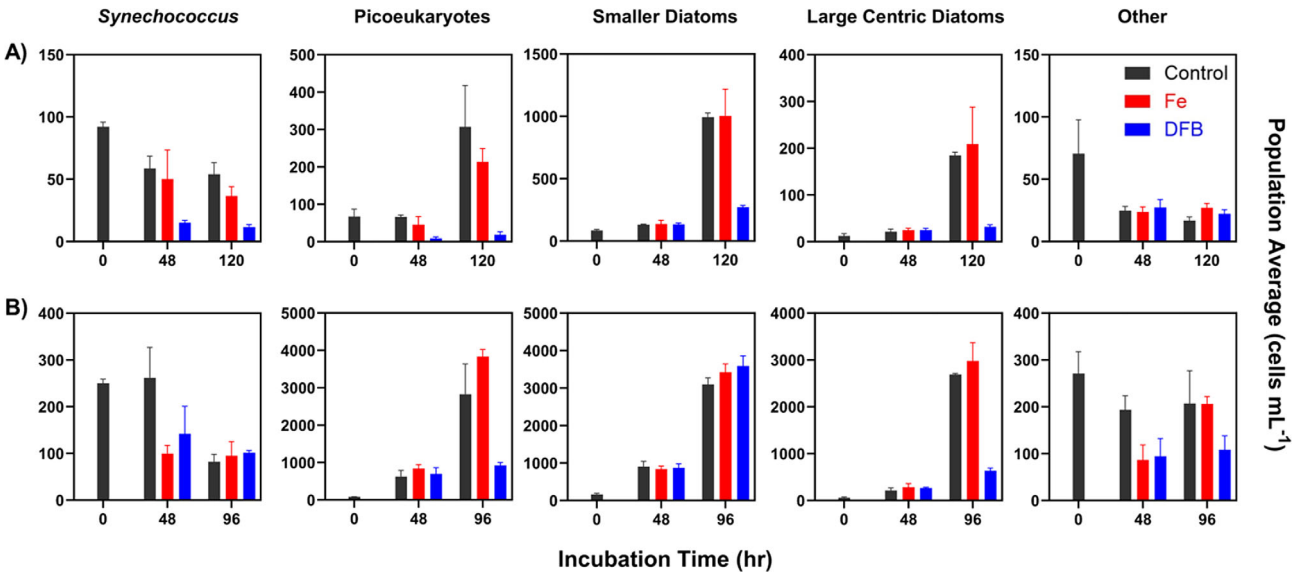

Fig. 3. FCM derived cell densities (cells mL^{-1}) at each incubation time (hours) of different phytoplankton populations in response to the control, Fe, or DFB treatments in the (**A**) wide shelf incubation experiment and (**B**) narrow shelf incubation experiment. Averages and standard deviations were measured from triplicate treatments. Gray, red, and blue bars represent population averages from control, Fe, and DFB treatments, respectively. Population averages for the initial seed community at T_0 are provided in Supplementary Table S1B. Growth rates derived from FCM counts of pico-eukaryotes, smaller diatoms (< 20 μm), and large centric diatoms (> 20 μm) are provided in Supplementary Table S2. Error bars represent the standard deviations of the mean ($n = 3$).

in the wide shelf incubations (Fig. 4A) were lower than the DIC ($0.0105 \pm 0.0023\ h^{-1}$) and nitrate uptake rates ($0.008 \pm 0.002\ h^{-1}$) in the narrow shelf incubations. For deep-water (T_0) phytoplankton < 5 μm, biomass-normalized DIC uptake (Fig. 4B) in the wide shelf incubation ($0.0013 \pm 0.0007\ h^{-1}$) was lower than that of the narrow shelf incubation (0.0044 ± 0.0013 h−1). Biomass normalized nitrate uptake rates for both the wide ($0.0041 \pm 0.002\ h^{-1}$) and narrow ($0.0036 \pm 0.0011\ h^{-1}$) shelf incubations were comparable in the small cell (< 5 μm) T_0 community. Absolute uptake DIC and nitrate uptake rates are discussed in the Supporting Information Fig. S4.

In the wide shelf incubation, biomass-normalized DIC and nitrate uptake rates of the larger phytoplankton (≥ 5 μm) did not exhibit significant differences among any treatment variable at T_1, but show accelerated growth by T_2 in the control and Fe treatments, while the DFB treatment exhibited considerably lower DIC uptake by T_2 (Fig. 4A). Additionally, nitrate uptake rates in the control and Fe treatment were significantly greater than that of the DFB treatment (Fig. 4C). In the narrow shelf incubation, biomass-normalized DIC uptake data suggest that DIC uptake rates were starting to plateau by T_2 in the large size-fraction (Fig. 4A). Interestingly, biomass-normalized nitrate uptake rates indicate a decline in nitrate uptake rate in the large size-fraction by T_2, in which the DIC uptake rates had also plateaued (Fig. 4C). For the small size-fraction, no noticeable Fe or DFB treatment effect on normalized nitrate uptake could be observed in the control (Fig. 4D).

Taxonomic composition

Taxonomic distribution based on normalized RNA transcript counts indicate diatom blooms under simulated upwelling in both incubations. The initial community in the wide shelf was comprised of a large proportion of dinoflagellates (47%) and other eukaryotes (35%), while diatoms (13%), chlorophytes (2%), and haptophytes (3%) were relatively low in abundance. However, diatoms represent a majority of the community in all treatments at T_1 (control: 47%; Fe: 77%; DFB: 51%) and T_2 (control: 69%; Fe: 88%; DFB: 60%), and Fe and DFB treatments had differential effects on their relative proportion throughout the incubation (Fig. 5A).

The initial community in the narrow shelf showed a stark contrast to that of the wide shelf in relative phytoplankton proportions, as there is a more even distribution of different phytoplankton taxa. Diatoms (29%) represent a higher proportion here compared to their counterparts in the wide shelf, while dinoflagellates (20%), haptophytes (11%), and chlorophytes (3%) comprise the rest of the main algal taxa. A large proportion of other eukaryotes (38%) could also be observed in the initial community (Fig. 5A). Diatoms similarly exhibit higher relative proportions in all treatments by T_1 (control: 71%; Fe: 73%; DFB: 56%) and T_2 (control: 80%; Fe: 82%; DFB: 62%), but the negative DFB treatment effect on their transcript abundances are more noticeable compared to the control and Fe treatments at both time points (Fig. 5A).

Within the diatom taxa, *Thalassiosira* species (42%) represented the highest proportion of diatoms in the initial

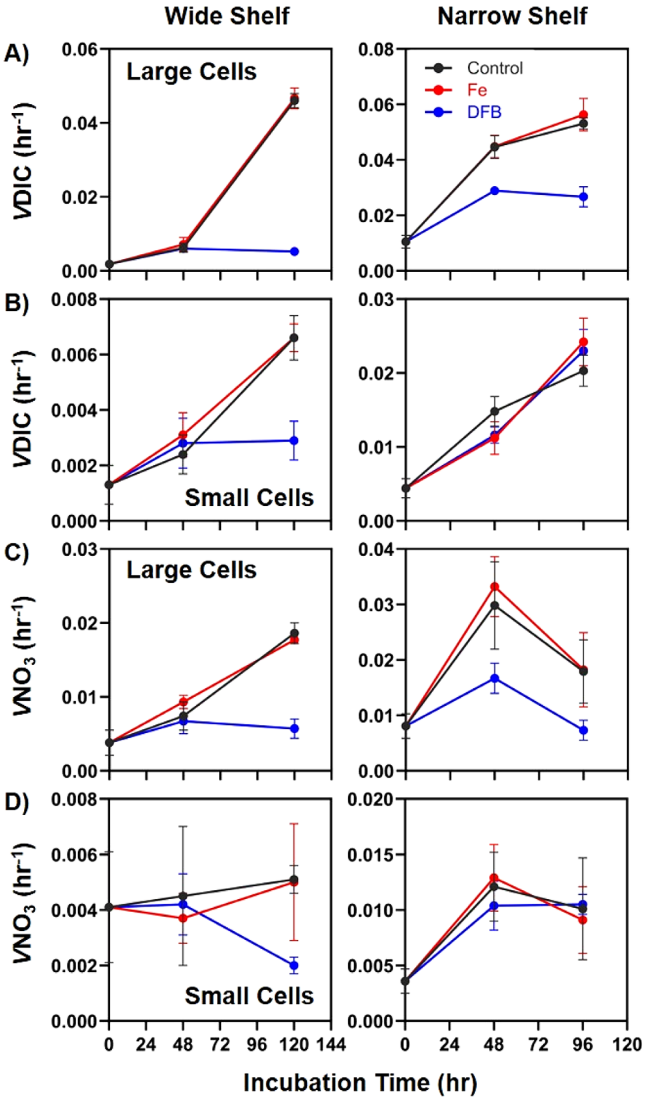

Fig. 4. Biomass-normalized (*V*) specific uptake rates of DIC in the (**A**) large cell size-fractions (≥ 5 μm) and (**B**) small cell size-fractions (< 5 μm), and biomass-normalized (*V*) specific uptake rates of nitrate (NO_3) in the (**C**) large cell size-fractions and (**D**) small cell size-fractions over the course of the incubation at the wide and narrow shelves. Biomass-specific uptake rates are normalized to respective particulate carbon and nitrogen within the size fractions and treatments. Black, red, and blue symbols and lines represent the control, Fe, and DFB treatments respectively. Error bars represent the standard deviations of the mean ($n = 3$).

community in the wide shelf, while the genera *Pseudo-nitzschia* (6%) and *Chaetoceros* (5%) were the next most abundant. By T_1 and T_2, *Thalassiosira* maintained high relative proportions in all treatments (Fig. 5B). Similarly, in the narrow shelf initial community, *Thalassiosira* show the highest relative proportions of any other diatom genera (24%), but only marginally, as initial populations of *Pseudo-nitzschia* (21%) and *Chaetoceros* (10%) exhibited higher relative abundance in the narrow shelf compared to the wide shelf. This relatively even distribution of diatom genera could be observed throughout the incubation in all treatments (Fig. 5B), with a noticeable effect on *Thalassiosira* relative abundance in the DFB treatment (24%) compared to the control (42%) and Fe (40%) at T_2. Contrastingly, at this same time point in the narrow shelf incubation, *Pseudo-nitzschia* seemed to respond positively to the DFB treatment (25%) and increased their relative abundance compared to the control (18%) and Fe treatments (15%). From our observations, while *Thalassiosira* (centric) diatoms responded positively to control and Fe treatments overall, *Pseudo-nitzschia* (pennate) diatoms seemed to thrive under Fe-limitation of the DFB treatment. Taxonomic distribution based on 18S ribosomal DNA are discussed in the Supporting Information Data (S1).

Phytoplankton gene expression

Normalized transcript abundances for the four major phytoplankton taxa (diatoms, dinoflagellates, chlorophytes, and haptophytes) indicate differential expression of Fe starvation, nitrogen assimilation, and photosynthesis genes between the Fe and DFB treatments and across T_0 (DW), T_1, and T_2 time points in both the wide shelf and the narrow shelf (Supporting Information Figs. S4, S7; Data S2.6). The three major diatom genera (*Pseudo-nitzschia*, *Chaetoceros*, and *Thalassiosira*) exhibited higher relative abundances of *ISIP1*, *ISIP3*, and *pTF* genes in DFB treatments throughout both incubations, but *ISIP1* expression was especially high in *Chaetoceros* and *Thalassiosira* at T_2 in the DFB treatment in the narrow shelf (Fig. 6B). Ferritin (*FTN*) was proportionally abundant in the *Pseudo-nitzschia* and *Thalassiosira* genera throughout the incubation at both wide and narrow shelves, but a noticeably lower transcript abundance of *Thalassiosira FTN* can be observed in the DW of the narrow shelf compared to *FTN* transcript abundance in the DW of the wide shelf, while *Pseudo-nitzschia FTN* transcript abundance maintained its relative proportions in the DW of both incubation experiments (Fig. 6). Nitrogen assimilation gene transcripts in both incubations were higher in abundance in the DW, control, and Fe treatments relative to the DFB treatments for *Pseudo-nitzschia* and *Thalassiosira*; NR was observed to be highly expressed in the DW relative to the rest of the incubation in *Pseudo-nitzschia* and *Thalassiosira* genera of both incubation experiments. The DFB treatment effect on nitrogen assimilation can be better distinguished at T_1 of both incubation experiments for all three diatom genera. Similarly, the gene encoding cytochrome b_6f complex Fe-sulfur subunit (*petC*) exhibited higher fold change in the control and Fe treatments relative to the DFB treatments in all three diatom genera. Overall, higher transcript abundances for various photosynthesis genes can be observed in the narrow shelf incubation experiments, especially in *Thalassiosira* genera (Fig. 6B).

Diatom rhodopsin genes (*RHO*) exhibited significantly increased expression in the DFB treatments at both time points in the narrow shelf (p-adj < 0.05). Diatom *ISIP1*, *ISIP3*,

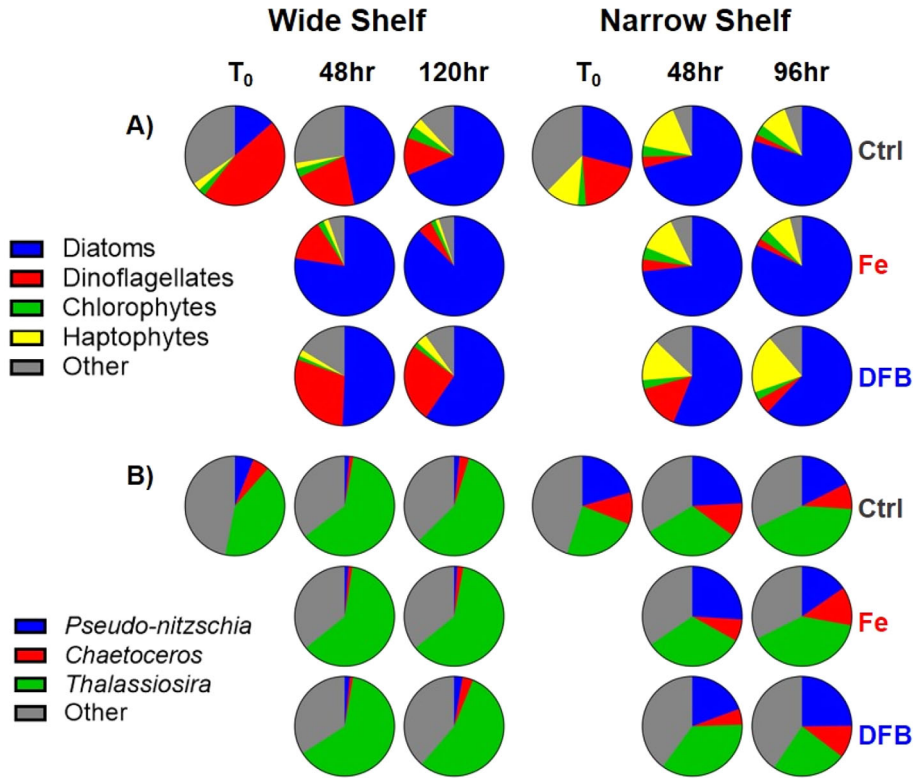

Fig. 5. Average taxonomic distribution by normalized mapped RNA reads from each time point (T_0: deep-water; T_1: 48 h; T_2: 120/96 h) and treatment (Control, Fe, and DFB, respectively). Taxonomic distributions are categorized as (**A**) percentage of mapped reads from the whole phytoplankton community and (**B**) percentage of mapped reads for the dominant diatom genera within all reads assigned and subset for diatoms (Bacillariophyta).

and *pTF* genes were significantly differentially expressed between the Fe and DFB treatments at both time points in the narrow shelf incubation, and at T_2 in the wide shelf incubation (p-adj < 0.05). *FTN* transcripts were also more abundant in the narrow shelf Fe treatments relative to the DFB treatments at both time points (p-adj < 0.05), but was not observed to be significantly differentially expressed in any of the wide shelf incubation time points (Fig. 7A). However, *FTN* was significantly expressed in the Fe treatment relative to the DW at T_2 in the wide shelf (Fig. 7A). Genes associated with the nitrate assimilation response of diatoms showed an inverse relationship with indications of DFB-induced Fe limitation in both of the incubations (Fig. 7). As observed, the relative expression of *NR* and *nirA* was significantly higher in the Fe treatments than those of the DFB treatments at T_2 for both incubations (p-adj < 0.05).

In both incubations, diatom photosynthesis genes were comparably highly expressed in the Fe treatments relative to the DFB treatments at T_2. Photosystem subunit genes (*psaB*, *psaE*, and *psaF*) were all found to be significantly expressed in the Fe treatment at either time points in the narrow shelf incubation, while the cytochrome b_6f complex genes (*petA*, *petB*, and *petC*) were significantly highly expressed only at T_2 in the narrow shelf incubation. Diatom differential expression of photosynthesis genes between the Fe and DFB treatments were observed in the wide shelf incubations at T_2, where *petC* increased in expression in the Fe treatment relative to the DFB treatment at both time points (Fig. 7A).

Discussion

Our findings suggest a larger initial biomass of the deep-water (T_0) community in the narrow shelf incubation likely played a role in shaping the enhanced physiological processes of the phytoplankton by the first time point of the incubation, while the smaller initial biomass of the wide shelf contributed to a slower response to the simulated upwelling. Furthermore, neither the wide nor narrow shelves exhibited Fe limitation on a physiological level, given that physiological data between the control and Fe treatments did not significantly differ throughout the incubations. However, significant physiological and molecular differences were observed between control and DFB and Fe and DFB treatments throughout both incubations. At the molecular level, we found that diatom nitrogen assimilation and photosynthetic genes were significantly highly expressed in the Fe treatments, while Fe-starvation indicating genes were significantly highly expressed in the DFB treatments. Furthermore, the comparison of the deep-water diatom communities between the wide and narrow shelves showcased significantly increased expression of the Fe-

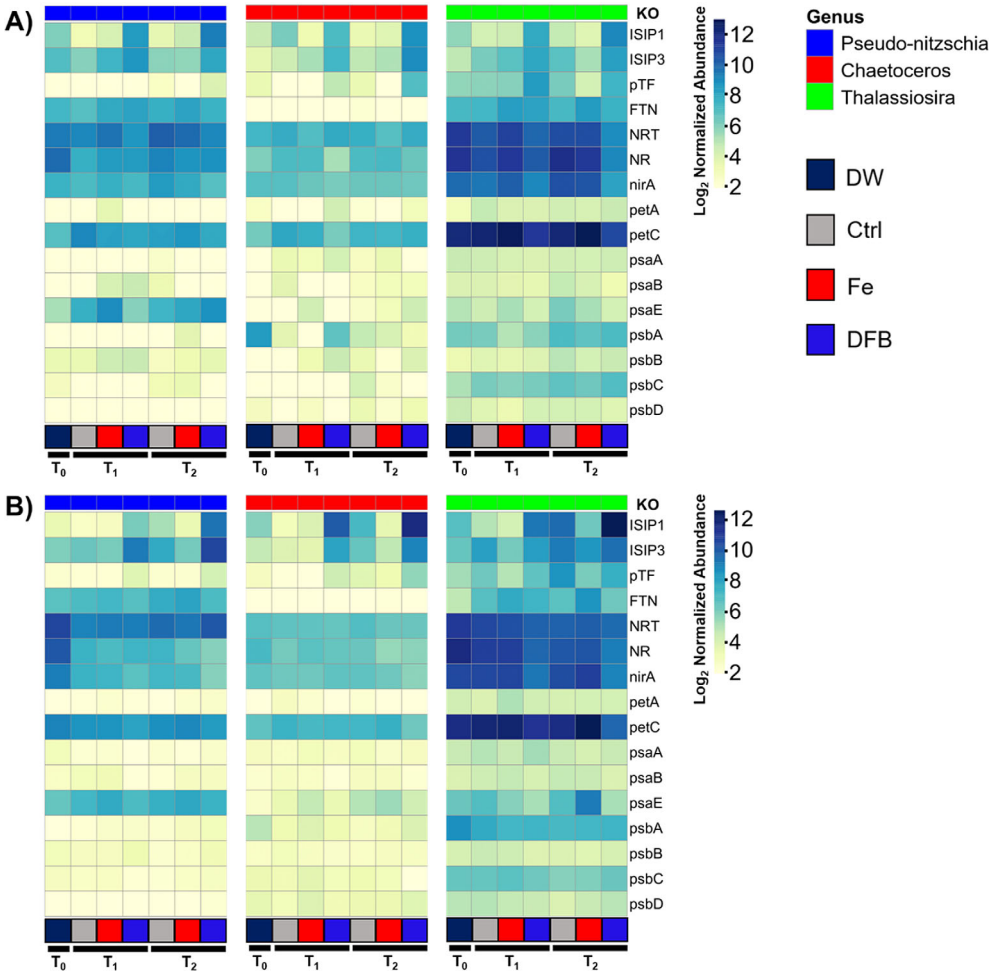

Fig. 6. Normalized transcript abundances of select iron homeostasis, nitrate assimilation, and photosynthetic genes identified among the three major diatom genera (*Pseudo-nitzschia*, *Chaetoceros*, and *Thalassiosira*) in the (**A**) wide shelf incubation (T_0 = DW, T_1 = 48 h, T_2 = 120 h) and (**B**) narrow shelf incubation (T_0 = DW, T_1 = 48 h, T_2 = 96 h). Abundances are normalized by total reads within each diatom genera. The bottom of each heatmap represents the respective treatment and timepoint of the three different genera. Deep-water at T_0 is denoted by DW, treatments at various time points are denoted by Ctrl, Fe, and DFB.

starvation induced protein 3 (*ISIP3*) indicator gene in the narrow shelf, suggesting the likelihood that Fe stress may have been occurring before it was observed on a physiological level.

Physiology and community composition changes due to simulated upwelling

Chl *a* concentrations at the second time point of both incubations suggest that the large cell fraction (≥ 5 μm) was almost an order of magnitude higher than that of the small cell fraction (< 5 μm). This is further substantiated by the phytoplankton taxonomic composition based on both normalized RNA and 18S rDNA read counts, where diatoms comprise a majority of the microalgal populations by the end in both the wide and narrow shelf incubations despite a minor presence in the respective initial deep-water communities. This is consistent with the concept that diatoms are known to dominate phytoplankton communities in coastal upwelling regions (Armbrust 2009; Malviya et al. 2016). Additionally, similarities in Chl *a* concentrations and DIC and NO_3 uptake rates in the control and Fe treatment indicate that neither communities in the wide shelf or the narrow shelf were experiencing Fe limitation on a physiological level in the initial stages of the simulated upwelling-induced phytoplankton blooms. Our Fe addition results corroborate various Fe fertilization experiments performed previously (Aumont and Bopp 2006; Coale et al. 1996). The DFB treatments, in which a strong organic chelator (i.e., siderophore) that binds to Fe was added (Kiss and Farkas 1998), were used to decrease Fe bioavailability. Interestingly, the dissolved Fe concentration measured from the same incubations was higher in concentration in the presence of the siderophore (Supporting Information Fig. S5). This is likely because DFB enhances Fe solubility and mediates the transfer of Fe from the particulate to the soluble pool (Segovia et al. 2017). However, Fe speciation plays an important role in

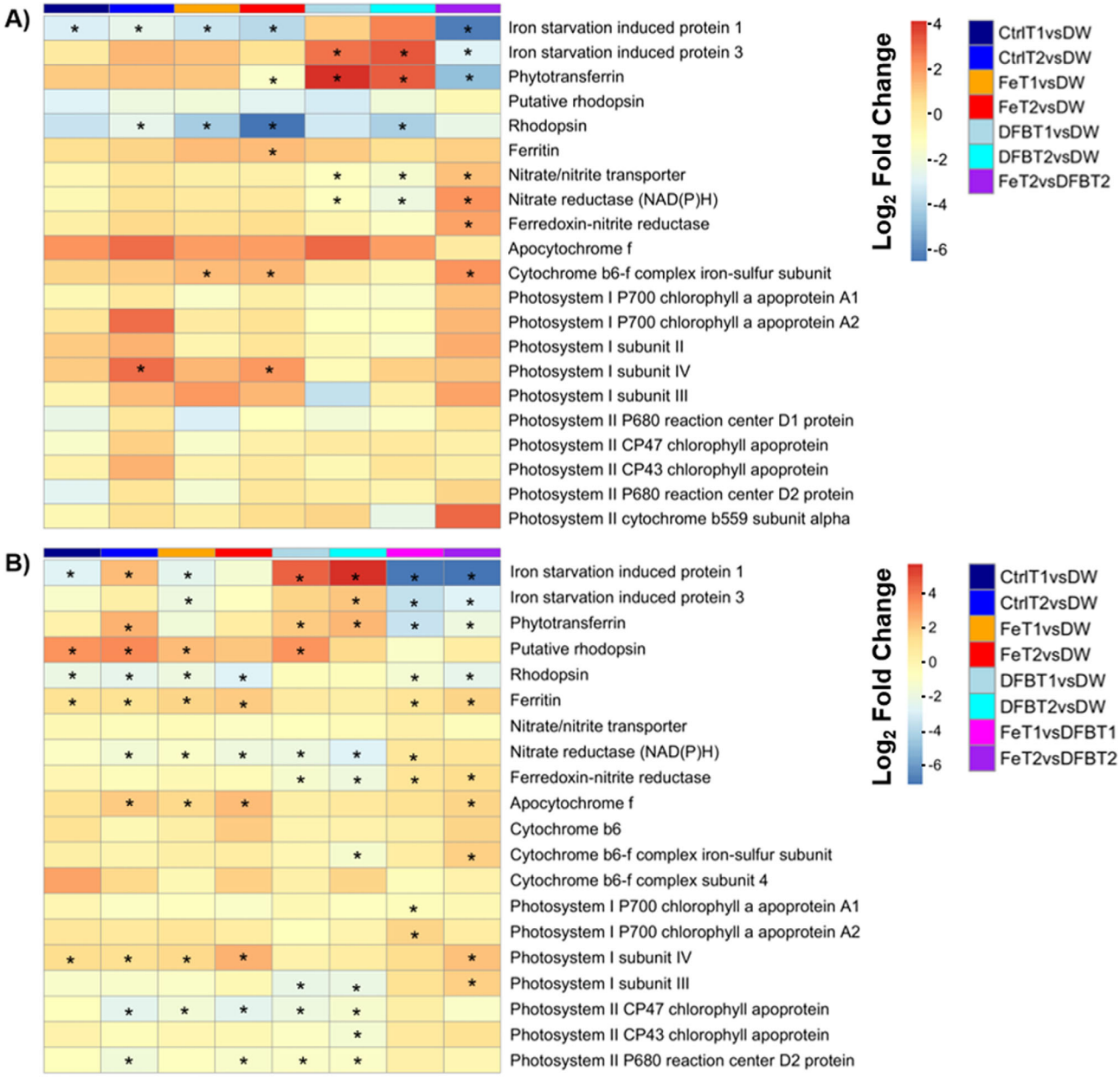

Fig. 7. Log_2 fold change of select iron homeostasis, nitrate assimilation, and photosynthetic genes between various treatment groups with respect to DW, T_1, and T_2 of (**A**) wide shelf diatoms and (**B**) narrow shelf diatoms. Significantly differentially expressed genes (log_2 fold change > 1 or < −1, *p*-adj < 0.05) are denoted by an asterisk (*).

Fe bioavailability in addition to dissolved Fe concentrations, and this Fe in the DFB treatments is likely not bioavailable because it is bound to the strong chelator. The DFB treatment resulted in expectedly lower phytoplankton growth rates and biomass accumulation relative to the control and Fe treatments in both incubations. Likewise, the addition of Fe or DFB differentially affected the physiology and growth kinetics of the larger phytoplankton, most evidently at the second timepoint.

Smaller diatoms in the narrow shelf appeared to sustain population growth despite the DFB treatment as indicated by fluorescence-assisted cell counts, suggesting the possibility that certain diatom genera may have been acclimated and/or buffered against low Fe conditions. This is substantiated by the taxonomic distribution of *Pseudo-nitzschia*, which sustained its RNA transcript and 18S rDNA abundances in spite of the DFB treatment at the second time point of the narrow shelf incubation, in contrast to *Thalassiosira*. One

explanation for this phenomenon could be that many pennate diatoms, especially *Pseudo-nitzschia*, can utilize the Fe-storage protein FTN during high Fe conditions to better buffer against episodes of low Fe and sustain growth when Fe becomes scarce (Yoshida et al. 2006; Marchetti et al. 2009; Sugie et al. 2011; Lampe et al. 2018). Likewise, the ability of *Pseudo-nitzschia* to continue cell divisions even under low dissolved Fe availability due to the presence DFB could suggest the use of such an Fe storage strategy. In contrast, many large centric diatoms that lack FTN will be unable to sustain growth in the low dissolved Fe availability, DFB treatment (Kustka et al. 2007). Interestingly, while deep-water communities of *Pseudo-nitzschia* maintained a relatively high abundance of *FTN* transcripts in both the wide and narrow shelves, *Thalassiosira* displayed a lower *FTN* transcript abundance in the deep-water of the narrow shelf. Ultimately, the viability of these smaller pennate diatoms under Fe limitation may have major implications for diatom composition shifts in future Fe-limited waters. In particular, *Pseudo-nitzschia* are known to produce domoic acid (Hasle 2002), a neurotoxin that may amplify in the food web through bioaccumulation and cause harm to humans and marine mammals alike. If indeed Fe limitation induces shifts in diatom composition toward *Pseudo-nitzschia* favorable conditions, the economic and environmental damage that these toxin-producing diatoms may impose in coastal regions could compound with various other climate change consequences.

Comparing across the incubations, the narrow shelf community exhibited higher phytoplankton biomass than the wide shelf community by approximately an order of magnitude across all treatments in the initial large cell size-fraction. Interestingly, rate processes continued in an upward trend in the wide shelf incubation as the cells were slowly acclimating to simulated upwelling; in contrast, large phytoplankton NO_3 uptake rates in the narrow shelf incubation appeared to be shifting down by the second time point. This is also supported by the differences in the macronutrient data compared across the two sites, where the drawdown of NO_3, PO_4, and $Si(OH)_4$ is more evident in the narrow shelf throughout the incubation. It was difficult to discern differences in macronutrient drawdown in the wide shelf incubation because there was slower biomass accumulation as a result of a low biomass initial seed population. Likewise, the larger initial seed community within the narrow shelf was able to rapidly increase growth in preparation for the simulated upwelling. Reasons behind the large seed population density at the narrow shelf are currently unknown, but a few explanations are considered in the Supporting Information Data (S2.10).

Diatom gene expression analysis

As inferred through both the physiology and gene expression data, Fe addition had a net positive effect on diatom growth compared to the DFB addition. The significantly increased expression of nitrogen assimilation genes (i.e., *NR* and *nirA*) and photosynthetic genes (i.e., *psaB*, *psaE*, *psaF*, *petA*, *petB*, and *petC*) in the Fe treatments substantiates the evidence that Fe-addition stimulates growth in phytoplankton through enhanced nitrogen assimilation and photosynthetic activity (Geider and La Roche 1994). Sensibly, Fe limitation directly impacts diatom photosynthetic efficiencies (Greene et al. 1991; Marchetti and Harrison 2007) and N assimilation rates (Timmermans et al. 1994), with notable reductions in both aspects of their growth. The increased expression of *ISIP1*, *pTF* (*ISIP2A*), *ISIP3*, and *RHO* genes in the DFB treatments of both incubations also corresponds to the noticeable decline in DIC and NO_3 uptake rates and biomass due to Fe limitation. These results are consistent with previous studies that have also observed increased *ISIPs* and *RHO* expression in diatoms to cope with Fe stress (Cohen et al. 2017; Behnke and LaRoche 2020). The significantly increased expression of *RHO* with respect to the DFB treatment could suggest the potential usage of an Fe-independent energy production/conservation strategy by diatoms under Fe limiting conditions (Marchetti et al. 2015; Andrew et al. 2023; Strauss et al. 2023). Although DFB is not necessarily a quantitative predictor of future Fe limitation, it does present a scenario of how declining Fe bioavailability can influence diatom physiology and gene expression. Siderophores are part of a vast quantity of organic ligands in the oceans that play vital roles in controlling trace metal bioavailability, and has been shown to negatively influence phytoplankton growth rates when present at high concentrations (Sanchez et al. 2018).

Comparing across the two incubation sites, there is a clear distinction in the timing of nitrogen assimilation activity between the wide and narrow shelves. Whereas the wide shelf diatoms differentially expressed nitrogen assimilation and photosynthetic genes at the second time point, the narrow shelf diatoms were able to differentially express nitrogen assimilation and photosynthetic genes at both time points, suggesting that the narrow shelf diatoms had already exhibited a response to Fe variability within 48 h, while the wide shelf diatoms were still acclimating to the simulated upwelling at the same time point. The significant differential expression of diatom *FTN* at both time points of the narrow shelf is not evident in the wide shelf incubation at either time points, and may be explained by the fact that *FTN* is associated with the luxury uptake of Fe, and thus has more consistent higher transcript abundance after cells have already undergone other photosynthetic metabolic processes (Marchetti et al. 2009). Therefore, it may be assumed that diatoms in the wide shelf were still building photosynthetic machinery through nitrogen assimilation, as indicated by their expression of *ATPase*, *NR*, and *nirA* in the wide shelf incubation relative to the narrow shelf incubation (Supporting Information Fig. S10). This would further reinforce our hypothesis that the larger seed population of diatoms in the narrow shelf was able to rapidly increase their growth during the simulated upwelling, while the smaller initial population

in the wide shelf took longer to acclimate and thus was still in a balanced growth phase during the second time point.

The differential expression of various Fe stress genes in the initial diatom communities of the wide and narrow shelves (Supporting Information Fig. S10) raises another question of what specifically is driving these molecular differences across the communities. One possibility may be that the narrow shelf seed community was advected through a horizontal undercurrent and contributed to the initial larger biomass. If that is the case, the previous community that was advected may have been undergoing a period of Fe limitation post bloom before reaching the area of collection, leading to the significantly increased expression of *ISIP3* and *psaE*. This differential expression could be explained by differences in diatom community composition across the two sites, but may also confirm previous evidence that the narrow shelf was more likely to be Fe-limited or entering a state of Fe limitation following the upwelling-induced phytoplankton bloom (Bruland et al. 2001). The abundance of *Pseudo-nitzschia* in the DFB treatment of the narrow shelf incubation is one exception to this trend, and may possibly be explained by their consistent expression of *FTN* transcripts in the deep-water population relative to the rest of the time points in the narrow shelf. Ultimately, *Pseudo-nitzschia* cells ability to sustain growth under Fe limitation may be attributed to the combined effects of the Fe-storage protein and the relatively lower demand and higher acquisition potential for Fe. Further experimentation and analysis should focus on examining transcriptional differences among the various diatom species that dominate these upwelling blooms, and verifying whether *FTN* has a significant effect on *Pseudo-nitzschia* success relative to the other diatoms. More attention on time histories of water masses could also help in our understanding of the differences in the physiological and molecular dynamics of these seed communities between the wide and narrow continental shelves.

Conclusions

Ultimately, this study was conducted with the aim to better understand complex upwelling systems. Nutrient uptake rates, community composition and gene expression data have been combined to show a differential response by phytoplankton to the upwelling conveyor belt cycle across the Fe limitation mosaic of the CCS. This topographical and biological variability within the CCS has affected a complex set of physical and biological interactions which shape the phytoplankton community structure and behavior in response to environmental changes. To address our central questions, we found that (1) Fe limitation significantly influences not only diatom bloom formation but also phytoplankton physiology, community structure, and gene expression. Fe-limited phytoplankton, especially larger-sized cells, exhibited slower growth rates and carbon and nitrogen-specific uptake rates under Fe-limitation. More specifically, (2) diatom gene expression showed differential patterns in response to Fe variability, where *ISIP* gene expression increased in DFB treatments, and *FTN* gene expression increased in Fe treatments. Furthermore, (3) seed populations play an important role in shaping the phytoplankton upwelling response and acclimation time. As observed, a phytoplankton seed population with larger biomass in the narrow shelf incubation resulted in a rapid biomass accumulation rate relative to that of the wide shelf incubation. Lastly, (4) the apparent ability to sustain growth by smaller phytoplankton—including smaller diatoms—under Fe limitation may cause major shifts in phytoplankton composition within coastal upwelling systems. Given that climate change could drastically alter phytoplankton assemblages in future oceans (Benedetti et al. 2021), this will have major implications for not only the food web but also global biogeochemical cycles. Thus, it is imperative for us to examine in further detail how environmental conditions can impact these dominant phytoplankton taxa, especially within an intricate and complex system such as the CCS, where future ocean change is projected to intensify the Fe limitation gradient between wide and narrow continental shelves.

Data availability statement

The data that support the findings of this study are publically available in NCBI at https://dataview.ncbi.nlm.nih.gov/object/PRJNA966115. Additional data for this project are also submitted to BCO-DMO under project number 768006.

References

Andrew, S. M., and others. 2023. Widespread use of proton-pumping rhodopsin in Antarctic phytoplankton. Proc. Natl. Acad. Sci. U. S. A. **120**: e2307638120.

Armbrust, E. V. 2009. The life of diatoms in the world's oceans. Nature **459**: 185–192.

Aumont, O., and L. Bopp. 2006. Globalizing results from ocean in situ iron fertilization studies. Global Biogeochem. Cycles **20**: 1–15. doi:10.1029/2005GB002591

Behnke, J., and J. LaRoche. 2020. Iron uptake proteins in algae and the role of Iron Starvation-Induced Proteins (ISIPs). Eur. J. Phycol. **55**: 339–360.

Benedetti, F., M. Vogt, U. H. Elizondo, D. Righetti, N. E. Zimmermann, and N. Gruber. 2021. Major restructuring of marine plankton assemblages under global warming. Nat. Commun. **12**: 6256.

Bruland, K. W., E. L. Rue, and G. J. Smith. 2001. Iron and macronutrients in California coastal upwelling regimes: Implications for diatom blooms. Limnol. Oceanogr. **46**: 1661–1674.

Capone, D. G., and D. A. Hutchins. 2013. Microbial biogeochemistry of coastal upwelling regimes in a changing ocean. Nat. Geosci. **6**: 711–717.

Carr, M.-E. 2001. Estimation of potential productivity in Eastern Boundary Currents using remote sensing. Deep Sea Res. Part II Top. Stud. Oceanogr. **49**: 59–80.

Closset, I., H. M. McNair, M. A. Brzezinski, J. W. Krause, K. Thamatrakoln, and J. L. Jones. 2021. Diatom response to alterations in upwelling and nutrient dynamics associated with climate forcing in the California current system. Limnol. Oceanogr. **66**: 1578–1593.

Coale, K. H., and others. 1996. A massive phytoplankton bloom induced by an ecosystem-scale iron fertilization experiment in the equatorial Pacific Ocean. Nature **383**: 495–501.

Cohen, N. R., and others. 2017. Diatom transcriptional and physiological responses to changes in iron bioavailability across ocean provinces. Front. Mar. Sci. **4**: 1–20. doi:10.3389/fmars.2017.00360

Crawford, D. W., and others. 2003. Influence of zinc and iron enrichments on phytoplankton growth in the northeastern subarctic Pacific. Limnol. Oceanogr. **48**: 1583–1600.

Falkowski, P. G. 1997. Evolution of the nitrogen cycle and its influence on the biological sequestration of CO2 in the ocean. Nature **387**: 272–275.

Geider, R. J., and J. La Roche. 1994. The role of iron in phytoplankton photosynthesis, and the potential for iron-limitation of primary productivity in the sea. Photosynth. Res. **39**: 275–301.

Gledhill, M., and K. N. Buck. 2012. The organic complexation of iron in the marine environment: A review. Front. Microbiol. **3**: 69.

Greene, R. M., R. J. Geider, and P. G. Falkowski. 1991. Effect of iron limitation on photosynthesis in a marine diatom. Limnol. Oceanogr. **36**: 1772–1782.

Hasle, G. R. 2002. Are most of the domoic acid-producing species of the diatom genus *Pseudo-nitzschia* cosmopolites? Harmful Algae **1**: 137–146.

Hutchins, D. A., G. R. DiTullio, Y. Zhang, and K. W. Bruland. 1998. An iron limitation mosaic in the California upwelling regime. Limnol. Oceanogr. **43**: 1037–1054.

Hutchins, D. A., and P. W. Boyd. 2016. Marine phytoplankton and the changing ocean iron cycle. Nat. Clim. Chang. **6**: 1072–1079.

Huyer, A. 1983. Coastal upwelling in the California current system. Prog. Oceanogr. **12**: 259–284.

Kiss, T., and E. Farkas. 1998. Metal-binding ability of desferrioxamine B. J. Inclusion Phenom. Mol. Recognit. Chem. **32**: 385–403.

Kustka, A. B., A. E. Allen, and F. M. M. Morel. 2007. Sequence analysis and transcriptional regulation of iron acquisition genes in two marine diatoms1. J. Phycol. **43**: 715–729.

Lampe, R. H., and others. 2018. Divergent gene expression among phytoplankton taxa in response to upwelling. Environ. Microbiol. **20**: 3069–3082.

Lampe, R. H., G. Hernandez, Y. Y. Lin, and A. Marchetti. 2021. Representative diatom and Coccolithophore species exhibit divergent responses throughout simulated upwelling cycles. mSystems **6**: 6. doi:10.1128/mSystems.00188-21

Malviya, S., and others. 2016. Insights into global diatom distribution and diversity in the world's ocean. Proc. Natl. Acad. Sci. U. S. A. **113**: E1516–E1525.

Marchetti, A., and P. J. Harrison. 2007. Coupled changes in the cell morphology and elemental (C, N, and Si) composition of the pennate diatom pseudo-nitzschia due to iron deficiency. Limnol. Oceanogr. **52**: 2270–2284.

Marchetti, A., and others. 2009. Ferritin is used for iron storage in bloom-forming marine pennate diatoms. Nature **457**: 467–470.

Marchetti, A., D. Catlett, B. M. Hopkinson, K. Ellis, and N. Cassar. 2015. Marine diatom proteorhodopsins and their potential role in coping with low iron availability. ISME J. **9**: 2745–2748.

Marchetti, A., and M. T. Maldonado. 2016. Iron, p. 233–279. *In* M. A. Borowitzka, J. Beardall, and J. A. Raven [eds.], The physiology of microalgae. Springer International Publishing.

Margalef, R. 1978. Life-forms of phytoplankton as survival alternatives in an unstable environment. Oceanol. Acta **1**: 493–509.

Milligan, A. J., and P. J. Harrison. 2000. Effects of non-steady-state iron limitation on nitrogen assimilatory enzymes in the marine diatom *thalassiosira weissflogii* (BACILLARIOPHYCEAE). J. Phycol. **36**: 78–86.

Sanchez, N., E. A. Brown, Y. Olsen, O. Vadstein, J. L. Iriarte, H. E. Gonzalez, and M. Van Ardelan. 2018. Effect of Siderophore on Iron Availability in a Diatom and a Dinoflagellate Species: Contrasting Response in Associated Bacteria. Frontiers in Marine Science **5**: 1–15. doi:10.3389/fmars.2018.00118

Segovia, M., and others. 2017. Iron availability modulates the effects of future CO2 levels within the marine planktonic food web. Mar. Ecol. Prog. Ser. **565**: 17–33.

Strauss, J., and others. 2023. Plastid-localized xanthorhodopsin increases diatom biomass and ecosystem productivity in iron-limited surface oceans. Nat. Microbiol. **8**: 2050–2066.

Sugie, K., K. Kuma, S. Fujita, S. Ushizaka, K. Suzuki, and T. Ikeda. 2011. Importance of intracellular Fe pools on growth of marine diatoms by using unialgal cultures and on the Oyashio region phytoplankton community during spring. J. Oceanogr. **67**: 183–196.

Till, C. P., J. R. Solomon, N. R. Cohen, R. H. Lampe, A. Marchetti, T. H. Coale, and K. W. Bruland. 2019. The iron limitation mosaic in the California current system: Factors governing Fe availability in the shelf/near-shelf region. Limnol. Oceanogr. **64**: 109–123.

Turnšek, J., J. K. Brunson, T. J. Deerinck, M. Oborník, A. Horák, V. A. Bielinski11, and A. E. Allen. 2019. Phytotransferrin endocytosis mediates a direct cell surface-to-chloroplast iron trafficking axis in marine diatoms.

Towards Subcellular Proteomic Maps in Model Marine Diatoms 19.

Timmermans, K. R., W. Stolte, and H. J. W. de Baar. 1994. Iron-mediated effects on nitrate reductase in marine phytoplankton. Mar. Biol. **121**: 389–396.

Wilkerson, F. P., and R. C. Dugdale. 1987. The use of large shipboard barrels and drifters to study the effects of coastal upwelling on phytoplankton dynamics 1, 2. Limnol. Oceanogr. **32**: 368–382.

Yoshida, M., K. Kuma, S. Iwade, Y. Isoda, H. Takata, and M. Yamada. 2006. Effect of aging time on the availability of freshly precipitated ferric hydroxide to coastal marine diatoms. Mar. Biol. **149**: 379–392.

Acknowledgments

We are grateful for the crew and staff of the R/V Oceanus and their valuable assistance and support throughout the cruise. We also thank Dr. Ryan Paerl at North Carolina State University for providing us the BD FACS Melody Flow Cytometer to process our samples, and Brian Dreyer at University of California Santa Cruz for assistance with the ICP-MS analyses. Funding for the project was provided to A.M. from a National Science Foundation grant (OCE1751805). The trace metal analyses were supported with startup funds from California State Polytechnic University, Humboldt and Award #26844 from Research Corporation for Science Advancement's Cottrell Scholar Award to C.P.T.[1]

Conflict of Interest

None declared.

Submitted 12 June 2023
Revised 02 October 2023
Accepted 28 January 2024

Associate editor: Bingzhang Chen